ORIGINAL ARTICLE

pH/Temperature Responsive Curcumin-Loaded Micelle Nanoparticles Promote Functional Repair after Spinal Cord Injury in Rats via Modulation of Inflammation

Taibao Qian[1] · **Zhixiang Li**[1] · **Lijun Shang**[3] · **Sutao Huang**[3] · **Guanglin Li**[3] ·
Weiwei Zheng[2] · **Yingji Mao**[1,3]

Abstract

BACKGROUND: The formation of an inhibitory inflammatory microenvironment after spinal cord injury (SCI) remains a great challenge for nerve regeneration. The poor local microenvironment exacerbates nerve cell death; therefore, the reconstruction of a favorable microenvironment through small-molecule drugs is a promising strategy for promoting nerve regeneration.

METHODS: In the present study, we synthesized curcumin-loaded micelle nanoparticles (Cur-NPs) to increase curcumin bioavailability and analyzed the physical and chemical properties of Cur-NPs by characterization experiments. We established an *in vivo* SCI model in rats and examined the ability of hind limb motor recovery using Basso–Beattie–Bresnahan scoring and hind limb trajectory assays. We also analyzed neural regeneration after SCI using immunofluorescence staining.

RESULTS: The nanoparticles achieved the intelligent responsive release of curcumin while improving curcumin bioavailability. Most importantly, the released curcumin attenuated local inflammation by modulating the polarization of macrophages from an M1 pro-inflammatory phenotype to an M2 anti-inflammatory phenotype. M2-type macrophages can promote cell differentiation, proliferation, matrix secretion, and reorganization by secreting or expressing pro-repair cytokines to reduce the inflammatory response. The enhanced inflammatory microenvironment supported neuronal regeneration, nerve remyelination, and reduced scar formation. These effects facilitated functional repair in rats, mainly in the form of improved hindlimb movements.

CONCLUSION: Here, we synthesized pH/temperature dual-sensitive Cur-NPs. While improving the bioavailability of the drug, they were also able to achieve a smart responsive release in the inflammatory microenvironment that develops after SCI. The Cur-NPs promoted the regeneration and functional recovery of nerves after SCI through anti-inflammatory effects, providing a promising strategy for the repair of SCIs.

Keywords Spinal cord injury · Anti-inflammation · Nerve regeneration · Micelle

Taibao Qian and Zhixiang Li have contributed equally to this work.

✉ Yingji Mao
myj123@bbmc.edu.cn

1 Department of Orthopedics, First Affiliated Hospital of Bengbu Medical College, 287 Changhuai Road, Bengbu 233004, China

2 Department of Orthopaedics, The Affiliated Suzhou Hospital of Nanjing Medical University, Gusu School, Nanjing Medical University, 242 Guangji Road, Suzhou 215006, China

3 Anhui Province Key Laboratory of Tissue Transplantation and School of Life Sciences, Bengbu Medical College, 2600 Donghai Road, Bengbu 233030, China

1 Introduction

Spinal cord injury (SCI) is a neurodegenerative disease that can cause severe neurological deficits [1–3]. Impairment of sensory and motor functions imposes a significant burden on the quality of life of patients. After SCI, secondary pathological cascade changes, such as nerve cell death, axonal demyelination, infiltration of glial cells and macrophages, and microcyst formation, can hinder post-injury treatment [4]. Over the years, many animal models have been established and developed to study the mechanisms of SCI and functional recovery, as well as to evaluate potential therapeutic interventions [5–7]. Currently, effective treatments for SCI include neuroprotection and neuroregeneration. However, a prerequisite for neuroregeneration is to establish a favorable microenvironment. The strong inflammatory response that inevitably occurs following SCI not only causes nerve cell death but also leads to the formation of cavities and scarring, which is an important factor limiting neural regeneration. Related studies have confirmed that the inhibitory inflammatory microenvironment at the injury site supports the differentiation of astrocytes and hinders neuronal regeneration [8–10], challenging SCI repair. Therefore, a promising therapeutic strategy for neuronal regeneration is to regulate the inflammatory response after SCI and re-establish a microenvironment conducive to regeneration.

The inflammatory response contributes significantly to the disturbance of the microenvironment after SCI, and reducing the inflammatory response is of great importance for inhibiting apoptosis and maintaining neuronal survival. The body establishes a natural immune response in the early stages of SCI. Blood-derived immune cells infiltrate and transform into macrophages to participate in this immune process, along with microglia [11]. The neuroinflammatory response mediated by macrophages is influenced by lipopolysaccharide (LPS) and reactive oxygen species (ROS) [12, 13], and macrophages play an important role in the inflammatory response [14]. However, classically activated macrophages exhibit two polarization states, M1 and M2, and these polarization states play different roles in the inflammatory response. M1 macrophages are pro-inflammatory [15, 16], killing adjacent cells and inhibiting cell growth. They release inflammatory cytokines, such as TNF-α and IL-6, which can activate other inflammatory cells and accumulate them at the site of injury, resulting in an inflammatory cascade. In contrast, M2 macrophages can suppress the inflammatory response [14], which promotes cell activation and tissue growth and plays an active role in SCI repair. Therefore, regulating the polarization status of macrophages is beneficial to balance

the inflammatory microenvironment after SCI and to facilitate neuroregeneration through neuroprotection.

According to pathophysiology, a complex series of molecular events following SCI can lead to an intense inflammatory response at the injury site, which can affect nerve regeneration and repair. Anti-inflammatory drugs improve the inflammatory microenvironment by reducing the inflammatory effects after SCI, thus providing the basic conditions for nerve repair.

In the early stages of trauma, macrophages, as the main phagocytes in the inflammatory phase, exhibit the M1 pro-inflammatory phenotype and secrete pro-inflammatory cytokines and chemokines, such as IL-6, IL-1β, ROS, TNF-α, iNOS, etc. Subsequently, macrophages transition into the M2 anti-inflammatory phenotype, promoting repair through cell differentiation, proliferation, and matrix secretion as well as reorganization by secreting or expressing pro-repair cytokines, including TGF-β, Arg-1, IL-10, VEGF, etc.

Curcumin, a polyphenol extracted from natural plants, has antioxidant and anti-inflammatory activities [17, 18]. It can reduce inflammatory cell infiltration and promote conversion from M1 to M2 macrophages [19]. Thus, it has a positive effect on the regression of inflammation. Moreover, curcumin can inhibit neuronal apoptosis and improve myelin reformation for neuroprotective purposes, contributing to functional recovery after injury [20, 21]. After SCI, endogenous stem cells migrate to the injury site and differentiate into neurons. However, stem cell survival is limited in an inhibitory microenvironment, and neuronal transformation is less efficient. Related studies have shown that curcumin promotes the survival and proliferation of neural stem cells (NSCs), which is beneficial for repair after injury [22]. Owing to the synergistic effect of its anti-inflammatory properties, curcumin plays a positive role in SCI repair. After SCI, hemorrhage and edema at the injury site disturb local physiological activities, and the increase in anaerobic metabolic activity and inflammatory reaction increases the temperature and acidity at the injury site. An altered internal environment may affect the efficiency of drug utilization and prevent the drug from exerting its maximum pharmacological effect. Most importantly, curcumin is a water-insoluble substance, and an altered microenvironment reduces its bioavailability. To improve its bioavailability in a microenvironment with temperature and pH changes, we introduced a PNIPAM75-PLA60 block copolymer molecule that has dual pH/temperature sensitivity [23]. We constructed dual-sensitive micelle nanoparticles (NPs) with a hydrophilic outer layer and a curcumin-wrapped inner layer using the block copolymer molecule, which can improve hydrophilicity and at the

same time achieve better release through temperature and pH changes in the internal environment, greatly improving bioavailability. Meanwhile, the released curcumin exerts anti-inflammatory effects at the injury site, regulates the post-injury inflammatory microenvironment, achieves neuroprotection, and provides favorable conditions for nerve regeneration.

In this study, we explored the effect of curcumin-loaded micelle nanoparticles (Cur-NPs) on macrophage polarization in the inflammatory response and investigated neuronal regeneration and motor function recovery to confirm the positive effect and potential application of exogenous curcumin on SCI repair.

2 Materials and methods

2.1 Preparation of pH/temperature dual-sensitive NPs and Cur-NPs

The preparation of pH/temperature dual-sensitive Cur-NPs was carried out as described in the literature, with slight modifications [23, 24]. Initially, 20 mg of the PNIPAM75-PLA60 block copolymer compound (Polymersource, Canada) and 2 mg of curcumin (Sunlipo Biotech Research Center for Nanomedicine, Shanghai, China) were dissolved in 10 mL of dimethyl sulfoxide (DMSO, Solarbio, Beijing, China). Subsequently, the above solutions were mixed thoroughly, and 100 mL of deionized water was added to the mixed solution and stirred for several hours. Finally, the obtained mixture was dialyzed on a 1000 Da membrane overnight at 4 °C to obtain a curcumin-loaded nanoparticle system solution. The same method can be used to fabricate empty micelle NPs. The prepared nanoparticle system solution was stored at 4 °C for subsequent characterization.

2.2 Characterization of the pH/temperature dual-sensitive NPs

2.2.1 Transmission electron microscopy (TEM)

The morphological structures of the NPs and Cur-NPs were investigated using TEM (JEOL2010, Japan Electronics Co., Ltd., Japan). Briefly, the prepared solutions of NPs and Cur-NPs were diluted with deionized water in appropriate amounts, and then 10 μL of the dilutions were dropped onto the copper mesh of the carbon film, which was exposed to air at 26 °C to evaporate the water. The samples were then reverse-covered with 2% phosphotungstic acid (w/w) to fully infiltrate the staining. Finally, the samples were observed and photographed under a transmission electron microscope at 75 kV.

2.2.2 Release curve testing of the pH/temperature dual-sensitive Cur-NPs

We examined the release of Cur-NPs under different temperatures and pH conditions using slow-release experiments. First, 2 mL of the curcumin-loaded sensitive system solution (concentration blended to 0.4 mg/mL) was placed in a Millipore dialysis tube (dialysis molecular weight, 8–10 kDa), which was then sealed and placed in a beaker containing 1 L of phosphate-buffered saline (PBS, pH = 5.5 or 7.4) solution. The beaker was placed in a water bath shaker at 37 °C (shaking rate of 100 rpm). At set time points (1, 4, 8, 16, and 24 h), the dialysis tube was removed and 100 μL of carrier solution was aspirated into a 2 mL volumetric flask, to which acetonitrile was added to the scale and shaken well to lyse the lipids, followed by high-speed centrifugation at 1.5×10^4 rpm to obtain the supernatant. Finally, the supernatant was filtered through a 0.45-μm microporous membrane and detected by high-performance liquid chromatography (HPLC, Agilent 1220 Infinity II) at 430 nm [25–27]. Similarly, to determine the release of Cur-NPs at different temperatures, we adjusted the PBS solution to pH = 7.4 and then placed the beakers in a water bath shaker at 37 °C or 40 °C (shaking rate of 100 rpm). The subsequent experimental procedures were the same as those previously described. The above experiments were repeated three times to reduce experimental errors. The test parameters were: C18 column, 250 mm × 4.6 mm, 5 μm; mobile phase, acetonitrile-4.5% glacial acetic acid; flow rate, 1.0 mL/min; column temperature, 35 °C).

2.2.3 Drug loading efficiency

The drug loading efficiency of curcumin was determined using HPLC (Agilent 1220 Infinity II). In brief, the nano-solution carriers were prepared by the experimental method in the manuscript, and after freeze-drying, the mass of 2 mg was weighed precisely. We added 2 mL of acetonitrile to dissolve the lyophilized sample, and the supernatant was centrifuged at a high speed of 1.5×10^4 rpm. We injected 20 μL of the dissolved sample into HPLC after diluting with an appropriate amount of mobile phase and filtering, and the absorption peak at 430 nm was measured to utilize the drug loading capacity of curcumin in the carriers. Drug loading efficiency = amount of curcumin in the carrier/total mass of the drug carrier × 100%.

2.2.4 Fourier transform infrared (FTIR) spectroscopy

To detect infrared absorption peaks in the FTIR spectra of the samples, 10 mg of curcumin, NPs, and Cur-NPs mixed

with KBr powder were prepared and detected using an FTIR spectrometer (Nicolet iS5, Thermo Fisher, San Jose, CA, USA). Before detection, the wavelength range of the FTIR spectra was adjusted from 400 to 4000 cm^{-1}.

2.2.5 X-ray diffraction (XRD)

The crystal structures of curcumin, NPs, and Cur-NPs were analyzed using XRD. Briefly, 10 mg of curcumin, NPs, and Cur-NPs were added to the grooves of the slides, and the powder was uniformly covered on the surface of the grooves. Finally, the XRD patterns of the samples were obtained using an XRD analyzer (Rigaku Ultimate IV, Japan Rigaku Corporation, Japan). The parameters were set as follows: copper target, 1.5406 Å; voltage, 40 kV; current, 30 mA; scanning interval, 5–50°; and scanning speed, 10°/min.

2.2.6 Particle size and zeta potential

The size and potential distribution of the NPs were determined using photon correlation spectroscopy. Before detection, 10 mL of NPs and Cur-NPs solutions were diluted ten-fold at 26 °C to meet the detection requirements. Following addition to a quartz dish, the particle size distribution and zeta potential of the samples were measured using a Malvern laser particle sizer (Zetasizer Nano ZS, Malvern Instruments, Malvern, UK).

2.2.7 Establishment of the spinal cord contusion model and drug delivery

All animal experiments were approved by the ethics committee of Bengbu Medical College and conducted following the Chinese Ministry of Health and NIH guidelines for experimental nursing and utilization (Approval No. 2020238, Bengbu, China). Thirty adult female rats (weighing 220–250 g, purchased from Shushan District, Hefei, China) were housed in an animal room with a light/dark cycle (12/12 h). All rats were fed for 7 days in a room with controlled temperature and humidity for acclimatization. Food and water were withdrawn the day before surgery. The rat spinal cord contusion model was established using a New York University (NYU, New York) impactor, which has been reported in detail in previous studies [28]. Briefly, following intraperitoneal anesthesia with sodium pentobarbital solution (50 mg/kg), a 2 cm dorsal incision was made to expose the conus. This was followed by dorsal vertebral dissection at T8–T10, with no disruption of the dura to fully expose the spinal cord. Subsequently, the spines of T8 and T10 were clamped to stabilize the spine, and an impact injury was induced on the exposed dorsal surface of the spinal cord from a height of 15 mm using a 1.5 mm diameter metal impact bar weighing approximately 10 g. Successful modeling was indicated by twitching and tail wagging of the hind limbs in the rats. Finally, the spinal cord was delivered by direct drug injection using a stereotaxic microinjector. In the curcumin group (SCI rats treated with Cur-NPs), 0.2 mg was administered to each rat. The skin incision was sutured and disinfected after hemostasis. Post-surgery, the modeled rats were housed in an animal room at 26 °C and 40–60% humidity. To prevent infection, all operated rats were injected subcutaneously with antibiotics (2.0 mg/kg enrofloxacin 10%) for 5 days. During the first week post-surgery, urine was collected by manual bladder squeezing every 12 h until spontaneous urination resumed.

2.3 Behavioral analysis

2.3.1 Basso–Beattie–Bresnahan (BBB) score

The recovery of hindlimb motor function in rats after SCI was assessed using the BBB score, which is a scale score from 0 to 21 [29]. It was assessed by three independent observers, and the treatment was kept confidential. Hind limb function scores were analyzed weekly while the rats moved freely in the open field after surgery. Briefly, the rats were placed in an open field for free movement, and three observers assessed hind limb movements during locomotion. Scores were recorded between one and four weeks after surgery. Five rats were randomly selected from each group, and each experiment was repeated three times.

2.3.2 Hind limb trajectory

The visual state of hind limb movement in rats was assessed by the hind limb movement trajectory in the fourth week after SCI. Red and green dyes were used to label the untreated and curcumin-treated groups, respectively. The dye was applied evenly to the hind feet of each experimental rat, placed on the side of a rectangular groove lined with white paper, and allowed to crawl freely. Three rats in each group were selected to record the crawling trajectory for each test three times, and the crawling trajectory was photographed.

2.4 Enzyme-linked immunosorbent assay (ELISA)

We assessed the level of inflammation expression in rats by detecting inflammatory factors. Briefly, we collected serum from different groups of rats after the seventh day of SCI and measured the expression of TNF-α, IL-6, IL-4, and IL-10 according to the instructions of the ELISA kits (DAKEWEI, Guangzhou, China).

2.5 Immunofluorescence staining of spinal cord sections

Perfusion sampling was performed on each group of rats in the fourth postoperative week. First, 150 mL of PBS was used to intubate and perfuse the hearts of the rats, and then 150 mL of 4% paraformaldehyde was used to continue perfusion until the carcass became rigid. After separating the intact spinal cord from the trunk, a 2-cm long segment of the spinal cord was intercepted, centered on the injury, and fixed in 4% paraformaldehyde (PFA) for 24 h. The spinal cord was sequentially transferred to 20% and 30% sucrose for dehydration. Finally, the treated spinal cord was embedded in Tissue-Tek Optimal Cutting Temperature Compound (OCT, Sakura Finetek Japan Co., Ltd.) and sectioned on a cryostat (Leica, CM3050 S, Germany) at a thickness of 9 μm for subsequent immunofluorescence staining. Briefly, the treated sections were washed twice in PBS, and the spinal cord was closed with 10% donkey serum for 2 h. The sections were then incubated overnight with a diluted primary antibody. After washing three times in PBS, the sections were incubated with Cy3-coupled goat anti-rabbit and goat anti-mouse secondary antibodies (1:400; Affinity, Jiangsu, China) at 26 °C for 2 h. Finally, nuclear staining was performed with DAPI. The procedure was performed in a light-protected manner. After blocking, photographs were taken under a fluorescent microscope (Zeiss, Oberkochen, Germany), and the results were analyzed using ImageJ software (National Institutes of Health).

The primary antibodies used were as follows: β-III-tubulin (Tuj-1, rabbit, 1:400; Affinity), glial fibrillary acidic protein (GFAP, rabbit, 1:400; Affinity), MBP (rabbit, 1:400; Affinity), Tyrosine Hydroxylase (TH, 1:400, mouse; Abcam, Cambridge, UK), neurofilament (NF, 1:400, mouse; Abcam), and laminin (rabbit, 1:400; Abcam).

2.6 Statistical analysis

All data obtained were expressed as mean ± standard deviation and analyzed using SPSS (version 20.0; SPSS Inc., Chicago, IL, USA) and GraphPad Prism 8.0 (GraphPad Software). One-way analysis of variance and two-sample independent t-tests were used to compare the data between the groups. Statistical significance was set at $p < 0.05$.

3 Results

3.1 Physical and chemical characterization of NPs and Cur-NPs

The physical and chemical properties of the NPs are shown in detail in Fig. 1. The morphological structure of the NPs was analyzed using TEM.

As shown in Fig. 1A, both the NPs and Cur-NPs appeared spherical and possessed smooth surfaces. The diameter of both NPs was approximately 115 ± 8 nm, which was close to the size obtained by photon correlation spectroscopy.

Drug bioavailability is affected by the complex microenvironment after SCI. Therefore, it is vital to improve the application of drugs in harsh microenvironments after injury. The temperature and pH sensitivities of the Cur-NPs were tested using our slow-release experiment. As shown in Fig. 1B, when the temperature reached 37 °C, the release rate of the drug at pH 5.5 was much higher than that at pH 7.4 from the 4th hour onwards. At 24 h, the release rate of the drug at pH 5.5 was nearly 90%, which was much higher than that at pH 7.4 (50%). This indicates that an acidic environment is more likely to allow drug release at the same temperature. We also investigated the effects of different temperatures on the release rate of the drug under the same acidic conditions. As shown in Fig. 1C, at each time point of the assay, the rate at 40 °C was significantly higher than that at 37 °C. Most importantly, at the 16th hour, the release rate at 40 °C was almost complete, whereas that at 37 °C was 40%. This indicated that the release rate of drug-loaded NPs was higher in acidic and relatively high-temperature environments. This suggests that drug-loaded micelle NPs have pH/temperature dual-sensitivity, which fits with the microenvironment after SCI and facilitates the release of the drug to improve curcumin bioavailability.

The XRD results are shown in Fig. 1D. Curcumin showed several sharp crystal diffraction peaks at 13.6°, 16.2°, 19.6°, 29.7°, and 40.7°, indicating that free curcumin exists in the crystalline state. In contrast, the NPs and Cur-NPs showed broad diffraction peaks (12–45°). In addition, the Cur-NP showed a few crystal diffraction peaks at 17.8°, 21.5°, and 24°, but there was no overlap with the characteristic peaks of free curcumin, suggesting that curcumin was encapsulated in the nanopreparation as a crystalline molecule. The lack of overlap of the peaks of free curcumin and Cur-NPs could be the result of a shift in the peaks due to the action of molecular polymers.

The FTIR spectra of curcumin, NPs, and Cur-NPs are shown in Fig. 1E. The IR spectrum of curcumin showed characteristic absorption peaks at 3500 cm^{-1} for the
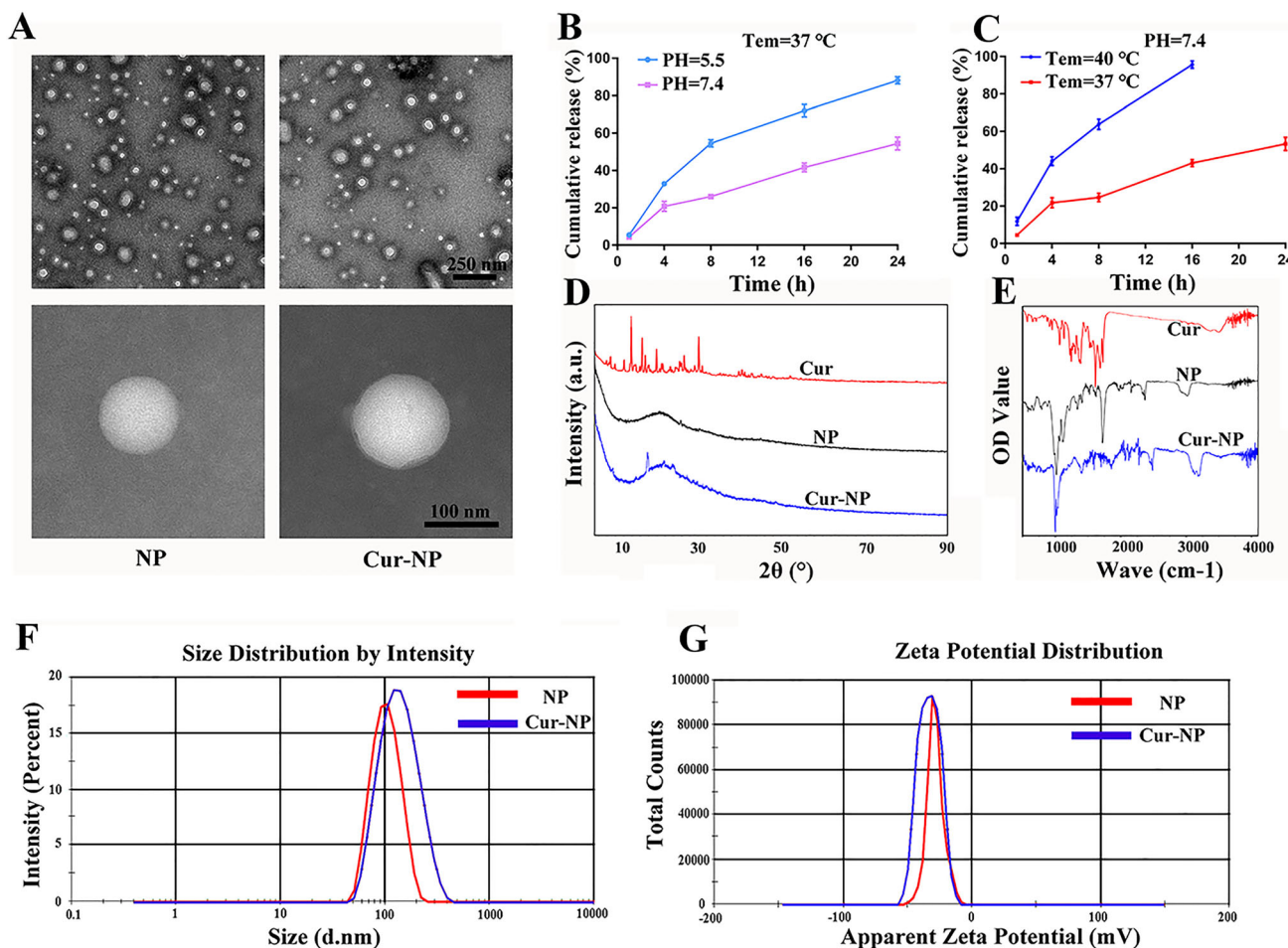
Fig. 1 Characterization of NPs and Cur-NPs. A TEM images of NPs and Cur-NPs. B The release of curcumin from micelle NPs at different pH conditions and time points (1, 4, 8, 16, and 24 h). C The release of curcumin from micelle NPs at different temperature conditions and time points (1, 4, 8, 16, and 24 h). D XRD spectroscopy analysis of free curcumin, NPs, and Cur-NPs. E FTIR spectroscopy detection of free curcumin, NPs, and Cur-NPs. F Zeta potential analysis of NPs and Cur-NPs. G The particle size distribution of NPs and Cur-NPs

stretching vibrations of –OH, 3300 cm^{-1} for the stretching vibrations of C–H, and 1625 and 1720 cm^{-1} for the stretching vibrations of the benzene ring and carbon–carbon double bonds, respectively. The NPs exhibited characteristic absorption peaks of amide N–H at 3000 cm^{-1} and C–O–C, C=O, and C–N structures at 1020, 1720, and 1120 cm^{-1}, respectively. The FTIR spectra of Cur-NPs both contained the –OH absorption characteristic peak of curcumin at 3500 cm^{-1} and the characteristic peaks of the amide group and C–O–C of the NPs, which indicated that curcumin was compatible with empty micelle-sensitive nanopreparations.

As shown in Fig. 1F, the diameters of the NPs and Cur-NPs were analyzed by dynamic light scattering. The diameters of the NPs and Cur-NPs were 107 ± 12 nm (polydispersity index = 0.087 ± 0.02) and 127 ± 14 nm (polydispersity index = 0.154 ± 0.01), respectively. For the zeta potential, the potentials of both NPs and Cur-NPs were between -40 mV and -30 mV (Fig. 1G), for which the presence of the potential caused the micelle NPs to be uniformly dispersed due to electrical repulsion. The negative zeta potential on the nanoparticle surface may be related to the block copolymer PNIPAM75-PLA60 [23]. The drug loading efficiency was calculated as $5.52 \pm 0.5\%$.

3.2 Application of Cur-NPs promotes hind limb movement in rats after SCI

Next, we examined the ability of Cur-NPs to repair SCI by evaluating hindlimb function, and hindlimb movement was assessed using the BBB score within four weeks after surgery. The BBB score was 21 for all animals before surgery, and the successful establishment of the SCI model

was demonstrated by a hind limb movement score of 0 for all groups of animals after surgery. As shown in Fig. 2A, functional repair of the hind limbs in the untreated SCI rats was not evident within four weeks after surgery. In contrast, the postoperative BBB scores of the rats in the curcumin-treated group were significantly improved. Two weeks post-operation, curcumin-treated rats showed a significant improvement in hind limb movement compared to untreated rats. In particular, the highest BBB score (approximately 12 points) was observed in week 4 after surgery. These results suggest that Cur-NPs have a significant therapeutic effect on SCI and promote functional recovery. At postoperative week 4, we also analyzed the gait trajectory of the hind limbs in the untreated SCI rats and curcumin-treated SCI rats. In Fig. 2B, we can observe that the SCI rats treated with Cur-NPs showed a more obvious footprint pattern, indicating that the rats were able to move their hind limbs through joint support. However, the untreated SCI rats dragged their hind limbs, indicating that the hind limbs did not have trunk support. This suggests that the application of Cur-NPs can promote hind limb motility in rats after SCI, which may be related to their ability to promote motor neuronal growth.

3.3 Cur-NPs promote macrophage polarization and reduce inflammatory responses in rats after SCI

The intense inflammatory response following SCI severely hinders nerve regeneration and repair. To investigate macrophage infiltration at the lesion site, immunofluorescence staining was performed at postoperative week 1 for CCR7 and ARG1. CCR7, a marker of M1 macrophages, plays a pro-inflammatory role in SCI. In contrast, ARG1, a marker of M2 macrophages, plays an anti-inflammatory role in SCI repair. As shown in Fig. 3A, B, positive staining for CCR7 and ARG1 was observed at the injury sites in both experimental groups. However, the number of ARG1-positive (M2) macrophages at the injury site was significantly higher in the curcumin-treated group than in the untreated SCI group. In contrast, the number of CCR7-positive (M1) macrophages in the treated group was lower than that in the untreated group. This indicated that a strong inflammatory response was generated after SCI and that M1 macrophages predominated at the injury site. The use of Cur-NPs could regulate macrophage polarization, causing a shift from M1 to M2 macrophages and eventually suppressing the inflammatory response after SCI, which provides a good microenvironment for nerve regeneration and injury repair.

The expression levels of inflammatory factors respond to the inflammatory situation of the organism. In the first week after SCI, the expression of pro-inflammatory factors TNF-α and IL-6 showed higher levels in the untreated group (Fig. 3E–F), while in the curcumin-treated group, we found that the expression of pro-inflammatory factors showed a decreasing trend, which might be because Cur-NPs affected the polarization of M2-type macrophages, thus inhibiting the secretion of inflammatory factors. As for some pro-repair cytokines, including IL-4 and IL-10, the curcumin-treated group showed a significantly higher trend of expression compared with the untreated group (Fig. 3G–H), which is beneficial for the repair of body tissues. Therefore, the use of Cur-NPs can promote the transformation of macrophages from the M1 to M2 phenotype, improve the inflammatory microenvironment by expressing pro-repair cytokines, and thus promote the repair of SCI.
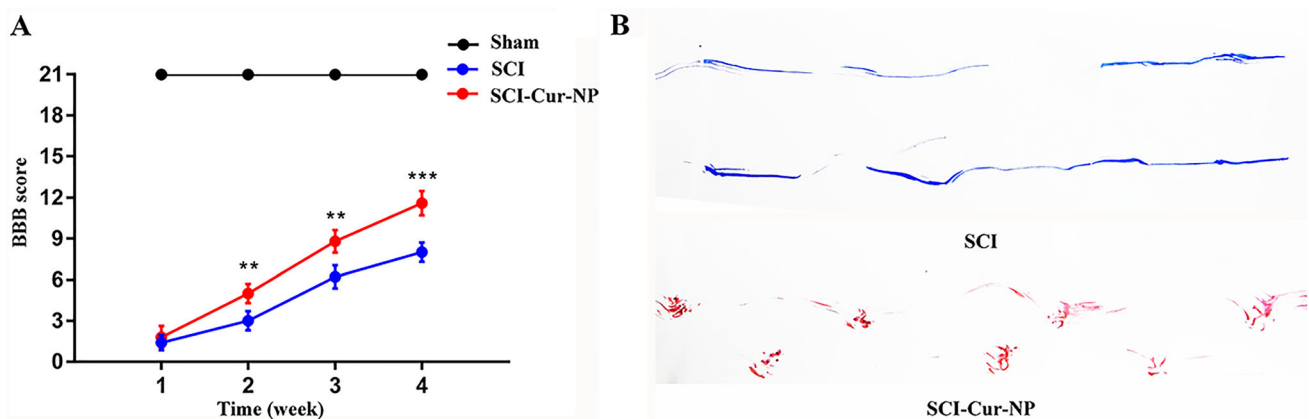
Fig. 2 Application of Cur-NPs promotes recovery of hindlimb movement and function in rats after SCI. **A** Detection of hindlimb motor function using BBB scores in rats at different time points 1–4 weeks postoperatively. **B** Trajectory analysis of hindlimb movement in rats at week 4 ($n = 5$ for each group, ** $p < 0.01$, *** $p < 0.001$, relative to the SCI group)
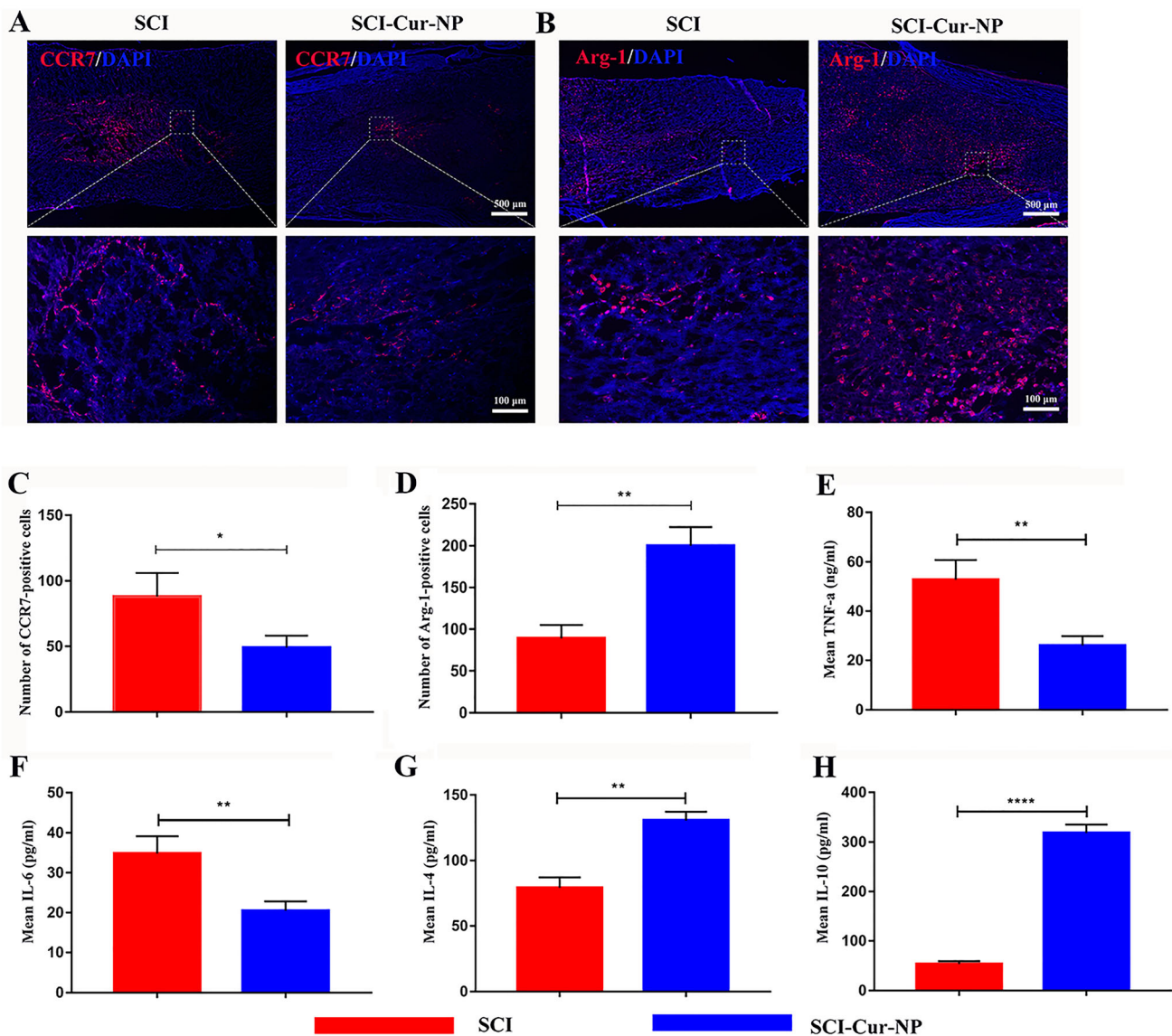
Fig. 3 Application of Cur-NPs promotes M2 macrophage polarization. **A** Representative images of immunofluorescence staining for M1 macrophages in different groups. **B** Representative images of immunofluorescence staining for M2 macrophages in different groups. **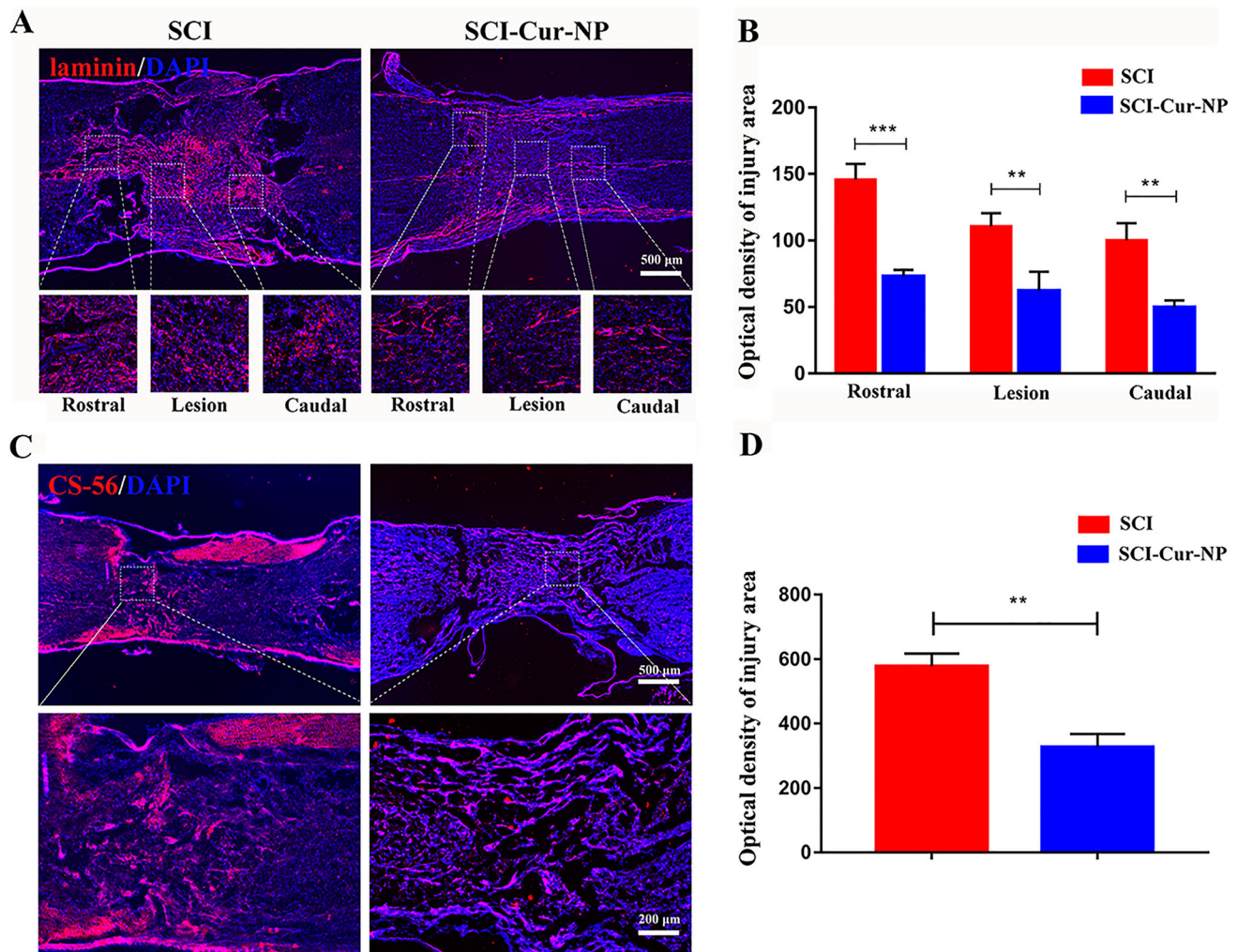C, D** Average immunofluorescence intensity analysis of M1 and M2 macrophage abundance in different groups. **E–H** Expression levels of TNF-α, IL-6, IL-4, and IL-10 in different groups 7 days after SCI ($n = 5$ for each group, $* p < 0.05$, $** p < 0.01$, relative to the SCI group)

3.4 Dual-sensitive Cur-NPs reduce glial scar formation in SCI rats

As a physical barrier to axonal regeneration, scar tissue significantly limits nerve regeneration. In this study, we used CS-56 and laminin immunofluorescence staining to label chondroitin sulfate proteoglycan and fibrous scars, respectively (Fig. 4). As for the fibrous scar fluorescence staining results (Fig. 4A), both the untreated and curcumin-treated groups presented laminin-positive staining at the injury site, indicating that SCI leads to scar formation. However, compared with the untreated SCI group, the curcumin-treated group demonstrated a significant decrease in the extent of fibrous scarring at the injury site of the rostral, lesion, and caudal regions. Most importantly, cavity formation was observed on both sides of the injury center in the untreated group, whereas no significant cavities were observed in the curcumin-treated group. The formation of cavities may be the result of intense inflammatory stimulation, and the application of Cur-NPs reduced the inflammatory response, thus protecting tissue repair by limiting the formation of cavities. The untreated group showed a large amount of CS-56 at the injury site, whereas the application of Cur-NPs reduced the amount (Fig. 4B).

Fig. 4 Cur-NPs can alleviate the formation of the restrictive outer matrix at the injury site. **A** Representative immunofluorescence images of fibrous scars at different injury sites in different groups. **B** Average fluorescence intensity analysis of fibrous scar at the injury site. **C** Representative images of CS-56 immunofluorescence in tissue sections at the injury site in different groups. **D** Average fluorescence intensity analysis of CS-56 at the injury site ($n = 5$ for each group, ** $p < 0.01$; *** $p < 0.001$, relative to the SCI group)

The immunofluorescence results were consistent. These results indicate that the application of Cur-NPs can effectively reduce the formation of scars associated with neuronal function and provide favorable conditions for nerve regeneration by regulating the poor microenvironment after injury.

3.5 Cur-NPs promote nerve cell regeneration and functional axon formation in SCI rats

It has been demonstrated that neurons differentiated from endogenous or exogenous NSCs after SCI can serve as connectors to facilitate electrophysiological activity at the injury site. We performed Tuj-1, GFAP, and MBP fluorescence staining to identify neuronal and glial cells at the injury site. The immunofluorescence staining results for the sections are shown in Fig. 5A. The curcumin-treated group

had significantly more Tuj-1-positive neuronal cells in the damaged spinal cord than the untreated group. Most importantly, neurons in the curcumin-treated group presented a continuous distribution at the upper and lower ends of the injury site. In contrast, the abundance of reactive astrocytes was significantly higher in the untreated group than in the curcumin-treated group (Fig. 5B), and the untreated group showed the formation of many cavities on both sides of the injury site, which also limited repair after SCI. Oligodendrocytes, with the ability to wrap around axons, play an important role in the formation of myelin sheaths and can assist in the transmission of bioelectrical signals. As shown in Fig. 5C, the positive expression of oligodendrocytes in the curcumin-treated group was significantly higher than that in the untreated group, which was more favorable for post-injury nerve regeneration and remyelination. Therefore, the application of Cur-NPs after
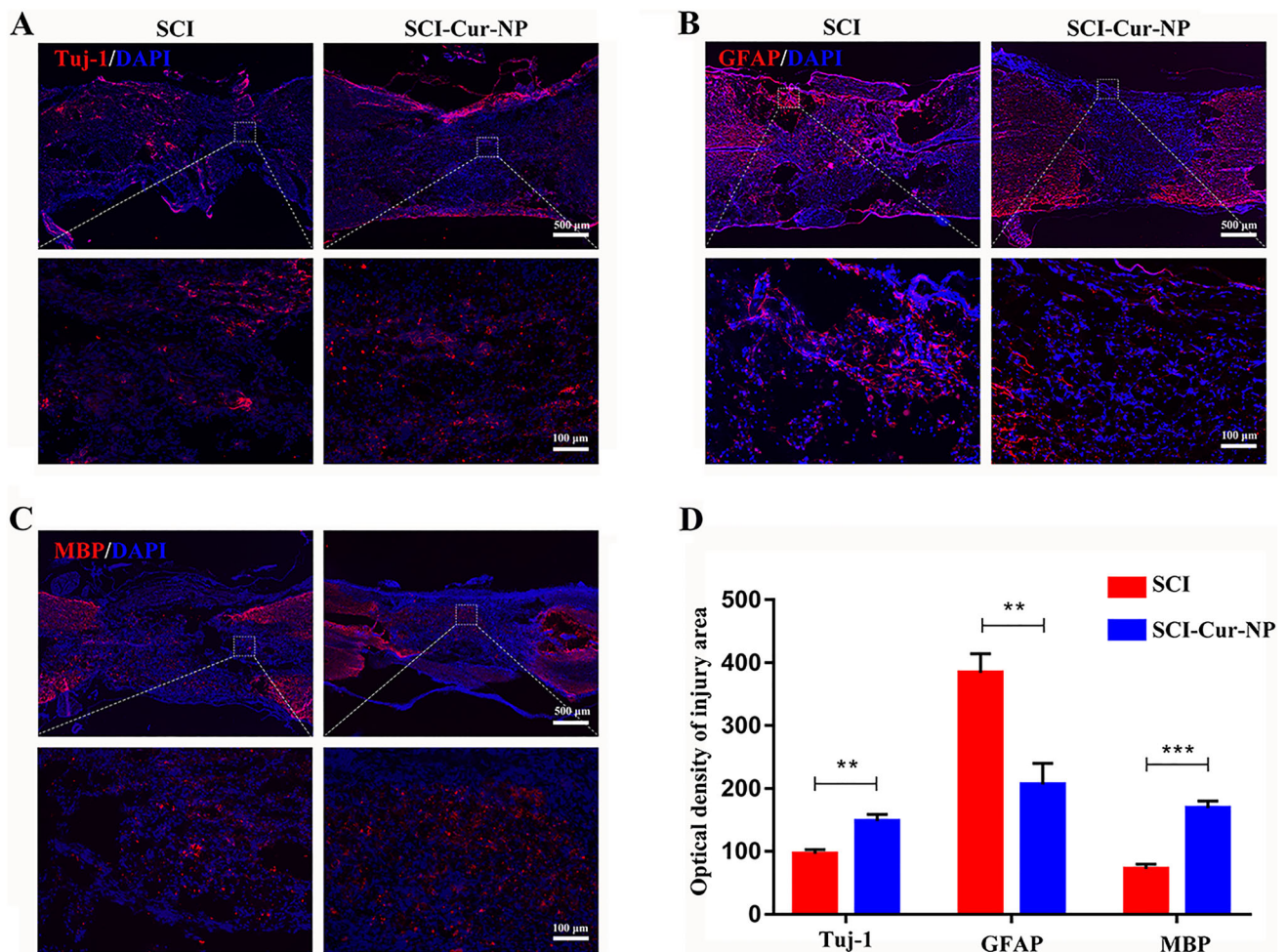
Fig. 5 Cur-NPs promote neuronal regeneration and remyelination and reduce astrocyte formation after SCI. **A–C** Representative immunofluorescence images of neurons, astrocytes, and oligodendrocytes at the site of injury in different groups after SCI. **D** Average fluorescence intensity analysis of neuronal, astrocyte, and oligodendrocyte abundance at the site of injury ($n = 5$ for each group, ** $p < 0.01$; *** $p < 0.001$, relative to the SCI group)

SCI is beneficial for promoting the growth of neurons and oligodendrocytes while reducing the production of astrocytes.

Serotonin (5-HT), catalyzed by TH (dopaminergic neuronal marker), is a neurotransmitter that plays an important role in motor function. Axonal regeneration is essential for spinal cord neural signaling during the injury phase, and NF-specific staining can be used as a biomarker for axonal repair. Therefore, immunofluorescence staining with NF and TH was performed to assess motor function and nerve regeneration. immunofluorescence results shown in Fig. 6 demonstrated that both positive NF and TH cells could be observed at the injury site at postoperative week 4. However, the curcumin-treated group showed more NF-positive axons than the untreated group (Fig. 6A). Most importantly, NF-positive cells in the curcumin-treated group showed continuous connections at the injury site, in contrast to the intermittent and scattered distribution of NF-

positive cells in the untreated group. The results of TH staining were similar to those of NF staining, and the number of TH-positive cells in the curcumin-treated group was significantly higher than that in the untreated group. These results suggest that the application of Cur-NPs promotes dopaminergic neuron growth, thereby facilitating the recovery of motor function. This fluorescence result is consistent with previous motor score results.

4 Discussion

A strong inflammatory response inevitably occurs after SCI, which causes nerve cell death and leads to the formation of cavities and scarring. This inflammatory microenvironment hinders neural regeneration. Therefore, regulating the inflammatory response after SCI and re-establishing a microenvironment conducive to regeneration
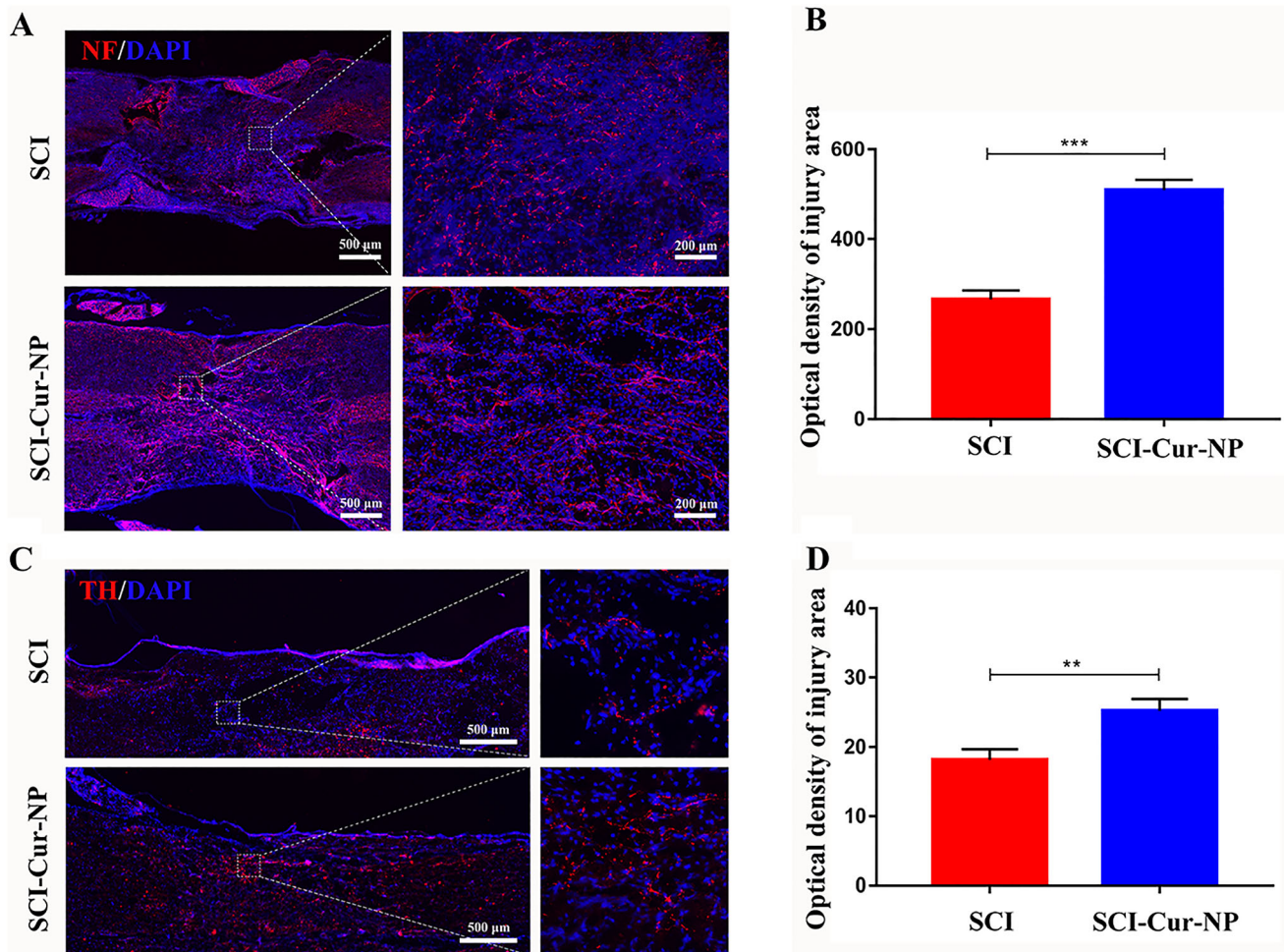
Fig. 6 Cur-NPs promote functional neuronal regeneration after SCI. **A** Representative images of NF immunofluorescence in tissue sections after SCI. **B** Average immunofluorescence intensity analysis of NF-positive cell abundance at the injury site. **C** Representative images of TH immunofluorescence in tissue sections after SCI. **D** Average immunofluorescence intensity analysis of TH-positive cell abundance at the injury site ($n = 5$ for each group, **$p < 0.01$; ***$p < 0.001$, relative to the SCI group)

is a promising therapeutic strategy for neuronal regeneration. Curcumin has anti-inflammatory effects and promotes NSC survival and proliferation, which are beneficial for repair after injury. However, curcumin is a water-insoluble substance, and an altered microenvironment reduces its bioavailability. In this study, we synthesized pH/temperature dual-sensitive Cur-NPs to improve curcumin bioavailability and investigated their effects on SCI.

In vitro, characterization experiments revealed that Cur-NPs have enhanced bioavailability and enable an intelligent responsive release in the injury microenvironment. This property improves physiological effects. In addition, the immunofluorescence results of *in vivo* tissue sections demonstrated that Cur-NPs could regulate macrophage polarization and thus exert anti-inflammatory effects, which is the initial and most critical stage of nerve repair. A favorable microenvironment provides favorable conditions for nerve regeneration and motor function recovery.

Furthermore, our findings demonstrated that intervention with Cur-NPs can significantly inhibit the activation of astrocytes after injury, reduce glial scar formation, and facilitate axonal regeneration in new nerve tissue. A certain amount of Cur-NPs was applied to a model of SCI, but the biosafety of these NPs is a more significant issue for us to consider. Relevant studies have shown that hydrogel scaffolds loaded with a certain amount of curcumin show good results in the repair of SCI [30], and given the slow-release effect of nanomaterials and the encapsulation rate, we chose a safe bio-range amount for administration in this experiment, thus avoiding the effect of biotoxicity on animal survival.

A series of molecular events after SCI induces the development of an inflammatory response, and the harsh microenvironment following injury accelerates neuronal cell death relative to normal tissue. Moreover, hemorrhagic edema at the injury site is even more difficult for tissue

repair. The death of cells at the injury site and the formation of an ischemic and hypoxic environment lead to an increase in anaerobic cellular metabolism, which exacerbates the microenvironmental imbalance and decreases the pH level. The inflammatory response is characterized by redness, swelling, and heat in the body tissues, so a microenvironment with a lower pH and higher temperature than normal tissues is formed after SCI. The sensitivity curve release kinetics of Cur-NPs in this study showed that NPs have pH/temperature responsive properties, which fit exactly into the microenvironment formed after SCI. Therefore, the low pH and high-temperature environment promotes the release of the lipid-soluble drug curcumin to improve its efficiency.

After SCI, inflammation, and oxidative stress result in an imbalanced microenvironment, leading to the rapid death of a large number of cells in the neural tissue, accompanied by the invasion of immune and fibrotic cells [31, 32]. This is detrimental to injury repair. As one of the first activated inflammatory cells, macrophages play a crucial role in tissue repair and immunological balance in the injured inflammatory microenvironment [33–35]. However, macrophages in different polarization states have different physiological effects [36]. Pathological inflammatory conditions are usually associated with dynamic changes in macrophage activation, and the balance state of M1 and M2 macrophages, releasing pro-inflammatory and anti-inflammatory factors, respectively, influences the direction of inflammation [37]. Curcumin is a plant-derived drug with antioxidant, anti-inflammatory, and antifibrotic properties. Related studies have confirmed that curcumin can reduce inflammatory cell infiltration and promote M2 polarization [19, 38]. In the pre-inflammatory phase of SCI, macrophages, as the main phagocytes in the inflammatory phase, present an M1 pro-inflammatory phenotype and secrete pro-inflammatory cytokines. Subsequently, macrophages change from the M1 type to the anti-inflammatory, repair-promoting M2 type, which promotes cell differentiation, proliferation, matrix secretion, and reorganization by secreting or expressing pro-repair cytokines. The transformation of M1 macrophages to M2-type macrophages is called macrophage polarization. The phenotypic transformation of macrophages is crucial to the tissue regeneration process, and untimely M1 to M2 phenotypic transformation can cause excessive inflammation and hinder the tissue repair process. In this experiment, we determined the drug effects by detecting the phenotype of early macrophages at the site of injury. Immunofluorescence of spinal cord tissue sections demonstrated that the abundance of M2 macrophages was higher in the curcumin-treated group than in the untreated group, whereas the abundance of M1 macrophages was the opposite. This suggests that Cur-NPs can balance the M1/M2 macrophage

ratio, thus facilitating the alleviation of inflammation under pathological conditions. Other studies have demonstrated that Cur-NPs can improve airway inflammation by inhibiting NLRP3 inflammatory vesicles in macrophages. However, we need to further explore how curcumin modulates macrophage polarization and exerts anti-inflammatory effects.

The progression of inflammation is a complex physiological process, and curcumin may serve neuroprotective purposes through multiple mechanisms. In several studies, curcumin was shown to protect the spinal cord post-damage by inhibiting the NF-kB pathway or activating Nrf2 signaling through the modulation of antioxidant genes (e.g., HO-1) [39, 40]. In a model of cerebral ischemia–reperfusion, curcumin was also able to regulate the PI3K/Akt/mTOR and TLR4/p38/MAPK pathways to suppress inflammation [41]. In studies of Parkinson's disease, curcumin was also shown to suppress astrocyte proliferation, inhibit the activation of NF-kB, and release pro-inflammatory mediators [42]. These studies suggest that curcumin has a protective effect and provides theoretical guidance for neuroprotection.

Neuronal gene expression and myelin regeneration are key components of nerve regeneration. Neurons serve as relay stations at the injury site, connecting physiological signals above and below the injury level. Oligodendrocytes play an important role in myelin formation. However, the formation of astrocytes at the injury site is the main cause of glial scarring. After SCI, secondary cascade reactions are followed by blood–spinal cord barrier damage and inflammatory cell infiltration. To limit the spread of inflammation, glial cells form an endogenous barrier [43, 44], yet they act as a barrier to axonal regeneration. Therefore, it is essential to reduce glial scarring for nerve regeneration, remyelination, and the recovery of SCI function. In the present study, the abundance of neurons and oligodendrocytes was significantly higher in the curcumin-treated group than in the untreated SCI group, whereas astrocyte abundance showed a significant decrease in the treated group compared to the untreated group. These results suggest that curcumin can improve the adverse microenvironment after SCI and create conditions for nerve regeneration. Thus, the application of Cur-NPs not only improves the inflammatory microenvironment but also promotes nerve regeneration. Importantly, some studies have shown that curcumin promotes survival and NSC proliferation [22]. After SCI, endogenous NSCs are activated and involved in injury repair. The advantage of endogenous stem cells is that they offer safety and freedom from ethical restrictions compared to transplanted stem cells [45–47]. However, the inefficient differentiation of endogenous stem cells into neurons is affected by the inhibitory microenvironment, in which NSCs over-

differentiate into astrocytes, which are involved in glial scarring. However, the anti-inflammatory and proliferation-promoting properties of curcumin greatly improve neuronal differentiation. NSCs are multipotent stem cells that can differentiate into neurons, astrocytes, and oligodendrocytes. Stem cells differentiate into neurons that can replace dead neurons and form new synaptic connections with the target cells. Differentiated oligodendrocytes can wrap around demyelinated or nascent axons to myelinate them during maturation, thus restoring the axonal signaling function. However, the restricted survival of stem cells in the inflammatory microenvironment after SCI coupled with inefficient neuronal transformation makes repair extremely difficult. Importantly, curcumin also promotes cell survival and proliferation in SCI [22], which is beneficial for repair after injury. Therefore, increased neuronal abundance in the curcumin-treated group was closely related to the involvement of endogenous stem cells. In addition, the recovery of motor function is the ultimate goal of SCI, and both TH and NF levels were significantly elevated in the curcumin-treated group. TH and NF regeneration is associated with the recovery of motor function, which is also why the application of Cur-NPs after SCI can promote motor function in the hind limbs of rats.

Therefore, the present study revealed that Cur-NPs may promote the recovery of hindlimb function in rats by inhibiting the inflammatory response after SCI, and this may be related to the regulation of macrophage polarization. This result has important implications for further studies investigating the repair mechanism of SCI at a later stage.

Authors contribution YM (Doctor of Philosophy) and WZ (Doctor of Medicine) were involved in the study design, literature research, data analysis, and writing the manuscript. TQ (Master of Medicine) and ZL (Master of Medicine) were involved in the study design, data analysis, and writing the manuscript. LS (Master of Medicine), SH (Master of Medicine), and GL (Master of Medicine) were involved in the data analysis.

Declarations

Conflict of interest The authors declare that there is no conflict of interest regarding the publication of this paper.

Ethical statement This study protocol was approved by the Institutional Animal Care and Use Committee (IACUC) of Bengbu Medical College (IACUC approval No. 2020238).

References

1. Jiang W, Li M, He F, Zhu L. Inhibition of NLRP3 inflammasome attenuates spinal cord injury-induced lung injury in mice. J Cell Physiol. 2019;234:6012–22.
2. Cowan H. Lakra C, Desai M. Autonomic dysreflexia in spinal cord injury. BMJ. 2020;371:m3596.
3. Li Z, Zhao T, Ding J, Gu H, Wang Q, Wang Y, et al. A reactive oxygen species-responsive hydrogel encapsulated with bone marrow derived stem cells promotes repair and regeneration of spinal cord injury. Bioact Mater. 2022;19:550–68.
4. Milich LM, Ryan CB, Lee JK. The origin, fate, and contribution of macrophages to spinal cord injury pathology. Acta Neuropathol. 2019;137:785–97.
5. Liu X, Mao Y, Huang S, Li W, Zhang W, An J, et al. Selenium nanoparticles derived from Proteus mirabilis YC801 alleviate oxidative stress and inflammatory response to promote nerve repair in rats with spinal cord injury. Regen Biomater. 2022;9:rbac042.
6. Li X, Fan C, Xiao Z, Zhao Y, Zhang H, Sun J, et al. A collagen microchannel scaffold carrying paclitaxel-liposomes induces neuronal differentiation of neural stem cells through Wnt/beta-catenin signaling for spinal cord injury repair. Biomaterials. 2018;183:114–27.
7. Kim DH, Cho HJ, Park CY, Cho MS, Kim DW. Transplantation of PSA-NCAM-positive neural precursors from human embryonic stem cells promotes functional recovery in an animal model of spinal cord injury. Tissue Eng Regen Med. 2022;19:1349–58.
8. Salewski RP, Mitchell RA, Li L, Shen C, Maria Milekovskaia M, Nagy A, et al. Transplantation of Induced pluripotent stem cell-derived neural stem cells mediate functional recovery following thoracic spinal cord injury through remyelination of axons. Stem Cells Transl Med. 2015;4:743–54.
9. Zhou P, Xu P, Guan J, Zhang C, Chang J, Yang F, et al. Promoting 3D neuronal differentiation in hydrogel for spinal cord regeneration. Colloids Surf B Biointerfaces. 2020;194:111214.
10. Deng W, Shao F, He Q, Wang Q, Shi W, Yu Q, et al. EMSCs build an all-in-one niche via cell-cell lipid raft assembly for promoted neuronal but suppressed astroglial differentiation of neural stem cells. Adv Mater. 2019;31:e1806861.
11. Beck KD, Nguyen HX, Galvan MD, Salazar DL, Woodruff TM, Anderson AJ. Quantitative analysis of cellular inflammation after traumatic spinal cord injury: evidence for a multiphasic inflammatory response in the acute to chronic environment. Brain. 2010;133:433–47.
12. Yuan Y, Chen Y, Peng T, Li L, Zhu W, Liu F, et al. Mitochondrial ROS-induced lysosomal dysfunction impairs autophagic flux and contributes to M1 macrophage polarization in a diabetic condition. Clin Sci (Lond). 2019;133:1759–77.
13. Li X, Wei Z, Wang X, Duan F, Xiong L, Li J, et al. Premna microphylla Turcz leaf pectin exhibited antioxidant and anti-inflammatory activities in LPS-stimulated RAW 2647 macrophages. Food Chem. 2021;349:129164.
14. Liu X, Zhang Y, Wang Y, Qian T. Inflammatory response to spinal cord injury and its treatment. World Neurosurg. 2021;155:19–31.
15. He L, Huang G, Liu H, Sang C, Liu X, Chen T. Highly bioactive zeolitic imidazolate framework-8-capped nanotherapeutics for efficient reversal of reperfusion-induced injury in ischemic stroke. Sci Adv. 2020;6:eaay9751.

16. Bloom O, Herman PE, Spungen AM. Systemic inflammation in traumatic spinal cord injury. Exp Neurol. 2020;325:113143.

17. Benzer F, Kandemir FM, Ozkaraca M, Kucukler S, Caglayan C. Curcumin ameliorates doxorubicin-induced cardiotoxicity by abrogation of inflammation, apoptosis, oxidative DNA damage, and protein oxidation in rats. J Biochem Mol Toxicol. 2018;32:e22030.

18. Jung KK, Lee HS, Cho JY, Shin WC, Rhee MH, Kim TG, et al. Inhibitory effect of curcumin on nitric oxide production from lipopolysaccharide-activated primary microglia. Life Sci. 2006;79:2022–31.

19. Wang F, Xia JJ, Shen LJ, Jiang TT, Li WL, You DL, et al. Curcumin attenuates intracerebral hemorrhage-induced neuronal apoptosis and neuroinflammation by suppressing JAK1/STAT1 pathway. Biochem Cell Biol. 2022;100:236–45.

20. Sanivarapu R, Vallabhaneni V, Verma V. The potential of curcumin in treatment of spinal cord injury. Neurol Res Int. 2016;2016:9468193.

21. Li W, Yao S, Li H, Meng Z, Su X. Curcumin promotes functional recovery and inhibits neuronal apoptosis after spinal cord injury through the modulation of autophagy. J Spinal Cord Med. 2021;44:37–45.

22. Chen Y, Yuan F, Lin J, Zhang X, Luo J, Huang L. Curcumin promotes the proliferation, invasion of neural stem cells and formation of neurospheres via activating SDF-1/CXCR4 axis. Folia Neuropathol. 2021;59:152–60.

23. Li W, Li J, Gao J, Li B, Xia Y, Meng, Y, et al. The fine-tuning of thermosensitive and degradable polymer micelles for enhancing intracellular uptake and drug release in tumors. Biomaterials. 2011;32:3832–44.

24. Nakayama M, Okano T. Polymer terminal group effects on properties of thermoresponsive polymeric micelles with controlled outer-shell chain lengths. Biomacromol. 2005;6:2320–7.

25. Sravani AB, Mathew EM, Ghate V, Lewis SA. A sensitive spectrofluorimetric method for curcumin analysis. J Fluoresc. 2022;32:1517–27.

26. Harigae T, Nakagawa K, Miyazawa T, Inoue N, Kimura F, Ikeda I, et al. Metabolic fate of poly-(lactic-co-glycolic acid)-based curcumin nanoparticles following oral administration. Int J Nanomedicine. 2016;11:3009–22.

27. Choi JS. Development of surface curcumin nanoparticles modified with biological macromolecules for anti-tumor effects. Int J Biol Macromol. 2016;92:850–9.

28. Duan FX, Shi YJ, Chen J, Ding SQ, Wang FC, Tang J, et al. Neuroprotective effects of P7C3 against spinal cord injury in rats. Exp Biol Med (Maywood). 2019;244:1680–7.

29. Basso DM. Beattie MS, Bresnahan JC. A sensitive and reliable locomotor rating scale for open field testing in rats. J Neurotrauma. 1995;12:1–21.

30. Luo J, Shi X, Li L, Tan Z, Feng F, Li J. An injectable and self-healing hydrogel with controlled release of curcumin to repair spinal cord injury. Bioact Mater. 2021;6:4816–29.

31. Norenberg MD, Smith J, Marcillo A. The pathology of human spinal cord injury: defining the problems. J Neurotrauma. 2004;21:429–40.

32. Sofroniew MV. Dissecting spinal cord regeneration. Nature. 2018;557:343–50.

33. Chawla A, Nguyen KD, Goh YP. Macrophage-mediated inflammation in metabolic disease. Nat Rev Immunol. 2011;11:738–49.

34. Dunster JL. The macrophage and its role in inflammation and tissue repair: mathematical and systems biology approaches. Wiley Interdiscip Rev Syst Biol Med. 2016;8:87–99.

35. Akilbekova D, Philiph R, Graham A, Bratlie KM. Macrophage reprogramming: influence of latex beads with various functional groups on macrophage phenotype and phagocytic uptake in vitro. J Biomed Mater Res A. 2015;103:262–8.

36. Kong X, Gao J. Macrophage polarization: a key event in the secondary phase of acute spinal cord injury. J Cell Mol Med. 2017;21:941–54.

37. Kotter MR, Setzu A, Sim FJ, Van Rooijen N, Franklin RJ. Macrophage depletion impairs oligodendrocyte remyelination following lysolecithin-induced demyelination. Glia. 2001;35:204–12.

38. Gao X, Han Z, Huang C, Lei H, Li G, Chen L, et al. An anti-inflammatory and neuroprotective biomimetic nanoplatform for repairing spinal cord injury. Bioact Mater. 2022;18:569–82.

39. Yardim A, Kandemir FM, Comakli S, Özdemir S, Caglayan C, Kucukler S. Protective effects of curcumin against paclitaxel-induced spinal cord and sciatic nerve injuries in rats. Neurochem Res. 2021;46:379–95.

40. Jin W, Wang J, Zhu T, Yuan B, Ni H, Jiang J. Anti-inflammatory effects of curcumin in experimental spinal cord injury in rats. Inflamm Res. 2014;63:381–7.

41. Huang L, Chen C, Zhang X, Li X, Chen Z, Yang C. Neuroprotective effect of curcumin against cerebral ischemia-reperfusion via mediating autophagy and inflammation. J Mol Neurosci. 2018;64:129–39.

42. Sharma N, Nehru B. Curcumin affords neuroprotection and inhibits alpha-synuclein aggregation in lipopolysaccharide-induced Parkinson's disease model. Inflammopharmacology. 2018;26:349–60.

43. Gaudet AD, Fonken LK. Glial cells shape pathology and repair after spinal cord injury. Neurotherapeutics. 2018;15:554–77.

44. Huang Y, Ren H, Gao X, Cai D, Shan H, Bai J, et al. Amlodipine improves spinal cord injury repair by inhibiting motoneuronal apoptosis through autophagy upregulation. Spine (Phila Pa 1976). 2022;47:E570–8.

45. Stenudd M, Sabelstrom H, Frisen J. Role of endogenous neural stem cells in spinal cord injury and repair. JAMA Neurol. 2015;72:235–7.

46. Zhang L, Fan C, Hao W, Zhuang Y, Liu X, Zhao Y, et al. NSCs migration promoted and drug delivered exosomes-collagen scaffold via a bio-specific peptide for one-step spinal cord injury repair. Adv Healthc Mater. 2021;10:e2001896.

47. Chen Z, Zhang H, Fan C, Zhuang Y, Yang W, Chen Y et al. Adhesive, stretchable, and spatiotemporal delivery fibrous hydrogels harness endogenous neural stem/progenitor cells for spinal cord injury repair. ACS Nano. 2022;16:1986–98.